Biophysical Chemistry 254 (2019) 106239

Contents lists available at ScienceDirect

Biophysical Chemistry

journal homepage: www.elsevier.com/locate/biophyschem

The pressure and temperature perturbation approach reveals a whole variety of conformational substates of amyloidogenic hIAPP monitored by 2D NMR spectroscopy

Markus Beck Erlach[a], Hans Robert Kalbitzer[a], Roland Winter[b], Werner Kremer[a,*]

[a] Institute of Biophysics and Physical Biochemistry, Center for Magnetic Resonance in Chemistry and Biomedicine, University of Regensburg, Universitätsstr. 31, 93053 Regensburg, Germany
[b] Physical Chemistry I- Biophysical Chemistry, Technical University Dortmund, Otto-Hahn-Str. 4a, 44227 Dortmund, Germany

HIGHLIGHTS

- Aim to understand the initial self-assembly of hIAPP
- Pressure and temperature induced NMR derived chemical shift changes pinpoint to structurally important residues
- Pressure and temperature dependencies reveal residues that seem to play an important role during aggregation
- Results show that the initial self-assembly of hIAPP diplays strong differences in comparison to Aβ

GRAPHICAL ABSTRACT

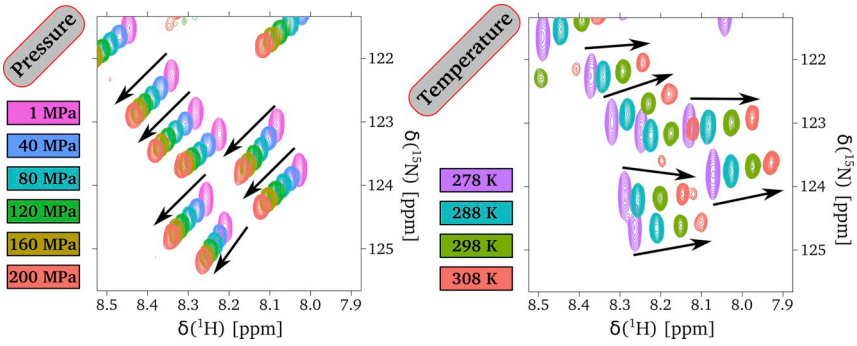

ARTICLE INFO

Keywords:
IAPP
Amylin
Amyloid
NMR
Fibrils

ABSTRACT

The intrinsically disordered human islet amyloid polypeptide (hIAPP) is a 37 amino acid peptide hormone that is secreted by pancreatic beta cells along with glucagon and insulin. The glucose metabolism of humans is regulated by a balanced ratio of insulin and hIAPP. The disturbance of this balance can result in the development of type-2 diabetes mellitus (T2DM), whose pathogeny is associated by self-assembly induced aggregation and amyloid deposits of hIAPP into nanofibrils. Here, we report pressure- and temperature-induced changes of NMR chemical shifts of monomeric hIAPP in bulk solution to elucidate the contribution of conformational substates in a residue-specific manner in their role as molecular determinants for the initial self-assembly. The comparison with a similar peptide, the Alzheimer peptide Aβ(1–40), which is leading to self-assembly induced aggregation and amyloid deposits as well, reveals that in both peptides highly homologous areas exist (Q10–L16 and N21–L27 in hIAPP and Q15–A21 and S26–I32 in Aβ). The N-terminal area of hIAPP around amino acid residues 3–20 displays large differences in pressure sensitivity compared to Aβ, pinpointing to a different structural ensemble in this sequence element which is of helical origin in hIAPP. Knowledge of the structural nature of the highly amyloidogenic hIAPP and the differences with respect to the conformational ensemble of Aβ(1–40) will help to identify molecular determinants of self-assembly as well as cross-seeded assembly initiated aggregation and help facilitate the rational design of drugs for therapeutic use.

* Corresponding author.
E-mail address: werner.kremer@ur.de (W. Kremer).

https://doi.org/10.1016/j.bpc.2019.106239
Received 19 June 2019; Received in revised form 26 July 2019; Accepted 26 July 2019
Available online 30 July 2019

1. Introduction

Proteins can generally and inherently exist in a variety of conformational substates under native-like conditions, and thus display conformational fluctuations, i.e., one protein molecule may reveal a whole number of conformational substates (CS) [1,2]. Identifying and studying these functionally relevant protein substates is generally not easy, since low fractional populated CS at ambient conditions are often not traceable [3]. As a result, many events in protein conformational dynamics possibly crucial and important for protein function, such as ligand binding and protein-protein interaction, stay completely undetectable [2,3]. The perturbation of the subpopulations by temperature and chemical means, such as small molecule compounds, are often used to offset the equilibrium populations and characterize the otherwise rare CS. Since some of the CS could only be separated by small energy differences, it may be difficult to achieve a separation by temperature or chemical perturbations. Vice versa, the third fundamental thermodynamic variable, pressure, can control the population of protein CS by affecting the dynamic equilibrium through volume differences with only minor energetic changes [3–10]. According to the principle of Le Châtelier, pressure favors states with smaller partial volumes. These are often more solvated than the native state through electrostriction, the hydration of newly exposed polar or non-polar residues, and the loss of cavities originating from packing defects in the folded ensemble of proteins. Many of these effects can be observed upon pressurization of proteins [3,8,10]. The application of high hydrostatic pressure (HHP) will populate low-lying excited CS which may be intimately involved in function since such states generally have a lower partial molar volume (see, e.g., Akasaka et al. [10]). HHP provides an elegant means to populate excited CS for spectroscopic studies, since HHP can be easily fine-tuned in the pressurization and depressurization direction, and its effects are generally reversible in biomolecular systems. Conformational selection postulates that the CS of proteins pre-exist in solution depending upon regions of the energy landscape (featuring several minima). These pre-existing CS may not always be easily detectable, however [11–13]. Many protein-ligand, protein-protein, and protein-nucleic acid interactions, where the binding of different partners leads to a population shift and thus redistribution of the already existing conformations, display features of conformational selection.

Here, we apply the pressure and temperature perturbation approach to gain insights into the CS of the human islet amyloid polypeptide (hIAPP), a highly amyloidogenic peptide. Our aim is to uncover the conformational states responsible for nucleation initiation leading subsequently to aggregation and finally amyloid formation of the polypeptide. The hormone hIAPP comprises 37 amino acids and is secreted by pancreatic beta cells along with glucagon and insulin. The glucose metabolism of humans is kept under control through a balanced ratio of insulin and hIAPP [14,15] and a disturbance can result in the development of type-2 diabetes mellitus. Depositions of extracellular amyloid in the pancreas where hIAPP is the main component are found in patients diagnosed with type-2 diabetes (T2DM). In pathological condition of T2DM, IAPP takes a fibrillar structure which is rich in cross-β-sheets. The triggering event for the conversion of native, soluble monomeric hIAPP into insoluble amyloid fibrils is still unclear. The amyloid fibril formation of synthetic hIAPP in bulk solution as well as in the presence of lipid membranes has been studied by various spectroscopic methods, but residue specific information of the native peptide is marginal.[15–23] Under physiological conditions, synthetic hIAPP remains soluble and displays an essentially random coil like structure as observed by circular dichroism (CD) and NMR spectroscopy [19–22]. However, Miranker and coworkers found also compact structures and a transient sampling of α-helical conformations [23]. Recent NMR investigations pointed to a potential role of the N-terminal region of hIAPP (residues 1–17) in the initial self-association of the peptide in bulk solution and not the known main amyloidogenic region (residues 20–29) of hIAPP [24]. However, the detection of the average conformational properties of native hIAPP did not reveal information about the existence of particular CS. Here we apply 2D NMR spectroscopy in combination with the pressure and temperature perturbation approach to uncover CS of hIAPP that are potentially prone to initiate the aggregation and subsequent fibrillation reaction. Multidimensional high-resolution NMR spectroscopy under high hydrostatic pressure is the most powerful technique to observe the structural properties at a residue specific level in solution and should be able to capture the pressure-induced transient species at the onset of the nucleation and aggregation process. Our findings could also be of significance for the optimization and search of inhibitors of hIAPP fibril formation [25,26], since it might provide structural information about the initial conformations prone to aggregation and fibril formation.

2. Materials and methods

2.1. NMR samples

Synthetic human ^{15}N-enriched islet amyloid polypeptide (hIAPP (1–37)) was obtained from Calbiochem (Germany), 1,1,1,3,3,3-hexafluoro-2-propanol (HFIP) from Riedel-de Haen (Germany). For the NMR measurements, the human islet amyloid polypeptide (hIAPP) was dissolved in HFIP to disperse potential aggregates, then lyophilized with an upstream cryogenic trap and resolved in 10 mM sodium acetate buffer (pH 5.5). DSS (4,4-dimethyl-4-silapentane-1-sulfonic acid) was added for referencing and $^{2}H_2O$ for the lock signal of the NMR spectrometer, resulting in the NMR sample containing 110 μM hIAPP(1–37), 10 mM Na-acetate buffer, pH 5.5, 0.1 mM DSS in 90% $^{1}H_2O$/10% $^{2}H_2O$.

2.2. NMR spectroscopy

NMR experiments were performed on a Bruker Avance 800 MHz NMR spectrometer operating at a ^{1}H frequency of 800.2 MHz. Measurements were performed in a 5 mm TCI cryo probe at temperatures of 278 K, 288 K, 298 K and 308 K. The absolute temperature inside the probe head was calibrated by measuring the chemical shift difference $\Delta\delta$ between the methyl and hydroxyl resonance of 100% methanol.[27] The ^{15}N chemical shifts were indirectly referenced to DSS [28].

2.3. High-pressure system

A homebuilt online-pressure system according to the Yamada-method [29] was used. Pressure was either produced by a homemade manually operated piston compressor or by an air-to-liquid-pressure intensifier (Barocycler® HUB440, Pressure BioSciences Inc., South Easton, MA, USA) controlled by the spectrometer. The pressure was transmitted via a high-pressure line (High Pressure Equipment Company, Linden, PA, USA) by methylcyclohexane or de-ionized water as pressurizing medium to the high-pressure ceramic cell (with an outer diameter of 5 mm and an inner diameter of 3 mm) from Daedalus Innovations LLC (Aston, PA, USA). The high-pressure cell was connected to the high-pressure lines by a titan autoclave developed in our laboratory [30]. The PBI Barocycler® HUB440 that controlled and monitored the output pressures was coupled via a microprocessor unit with the NMR spectrometer. In a Bruker Topspin auxiliary (AU) program, a user-defined set of high-pressure NMR experiments was started including an automated shimming of the sample after changing the pressure and before the actual experiment(s) were started. Pressure data were recorded from 0.1 MPa to 200 MPa in steps of 20 MPa.

2.4. Data evaluation

Data acquisition and processing was performed with Bruker TopSpin 3.2 PL6. For peak picking, the software AUREMOL [31] was

used. Data evaluation and fitting was done with the software package R [32].

The chemical shift values of the amide protons and nitrogen atoms in the [^{1}H-^{15}N] HSQC spectra under the influence of pressure were evaluated as described by Kremer et al. [33]. The data were first corrected for random-coil pressure effects by subtracting the known pressure dependence of the amino acid Xxx in the model peptide Ac-Gly-Gly-Xxx-Ala-NH_2 as published by Koehler et al. [34]. The obtained chemical shifts δ were then fitted to

$$\delta(p, T_0) = \delta_0(p_0, T_0) + B_1(p - p_0) + B_2(p - p_0)^2 \quad (1)$$

where δ_0 is the chemical shift at ambient pressure p_0, and B_1 and B_2 are the first and second order pressure coefficients. In addition the combined chemical shift δ_{comb} for corresponding ^{1}H and ^{15}N pairs were determined by the sum of the weighted chemical shifts δ(H) and δ(N) as described by Schumann et al. [35].

In contrast to the evaluation of the pressure effects, the data were examined with

$$\delta(T) = \delta_0 + C_1 T \quad (2)$$

where δ_0 is the chemical shift at 0 K and C_1 the linear temperature coefficient. As the pressure coefficients were corrected for the intrinsic pressure effect of each amino acid, the linear temperature coefficient C_1 was also corrected for the intrinsic temperature effect of each amino acid, leading to the corrected coefficient C_1^{corr}. The intrinsic temperature dependence for the amino acids were taken from Kjaergaard et al. [36] where the intrinsic temperature dependence of the amino acid Xxx was determined in the model peptide Ac-Gly-Gly-Xxx-Gly-Gly-NH_2.

The signal volumes, signal maximum intensities, and chemical shifts from the two-dimensional [^{1}H-^{15}N] HSQC spectra were analyzed using the AUREMOL software [31]. Both signal volumes and intensities at the signal maximum were corrected after Chen et al. [37] for the pressure dependence of the compressibility of water.

3. Results

3.1. Pressure dependence of the chemical shifts of hIAPP

Here we report the pressure and temperature induced changes of the chemical shifts in ^{15}N-enriched human IAPP(1–37) by [^{1}H-^{15}N] HSQC NMR spectroscopy. For this, we recorded a set of [^{1}H-^{15}N] HSQC spectra of hIAPP(1–37) at different pressures and temperatures (Fig. 1). The temperature was varied from 278 K to 308 K in steps of 10 K and the pressure was varied in steps of 20 MPa up to a final pressure of 200 MPa. The pressure dependence and signal intensities have been already described in Beck Erlach et al. [38].

The signal intensities of all recorded [^{1}H-^{15}N] HSQC spectra were calculated. The intensities of the signals at the different temperatures as a function of the applied pressure are shown in Fig. 2. The individual

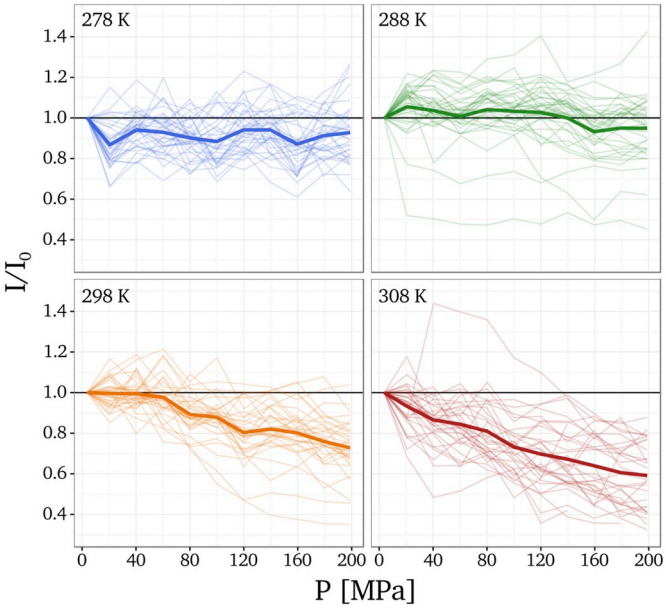

Fig. 2. Plot of the normalized relative intensities of all backbone NMR signals of hIAPP(1–37) derived from the [^{1}H-^{15}N] HSQC spectra recorded at different pressures in pressure steps of 20 MPa up to 200 MPa. Temperatures: 278 K (blue), 288 K (green), 298 K (orange), and 308 K (red). The sample contained 110 µM ^{15}N-enriched hIAPP(1–37) in 10 mM Na-acetate buffer, pH 5.5, 0.1 mM DSS in 90% ^1H_2O/10% ^2H_2O. Figure based on Beck Erlach et al.[38]. (For interpretation of the references to colour in this figure legend, the reader is referred to the web version of this article.)

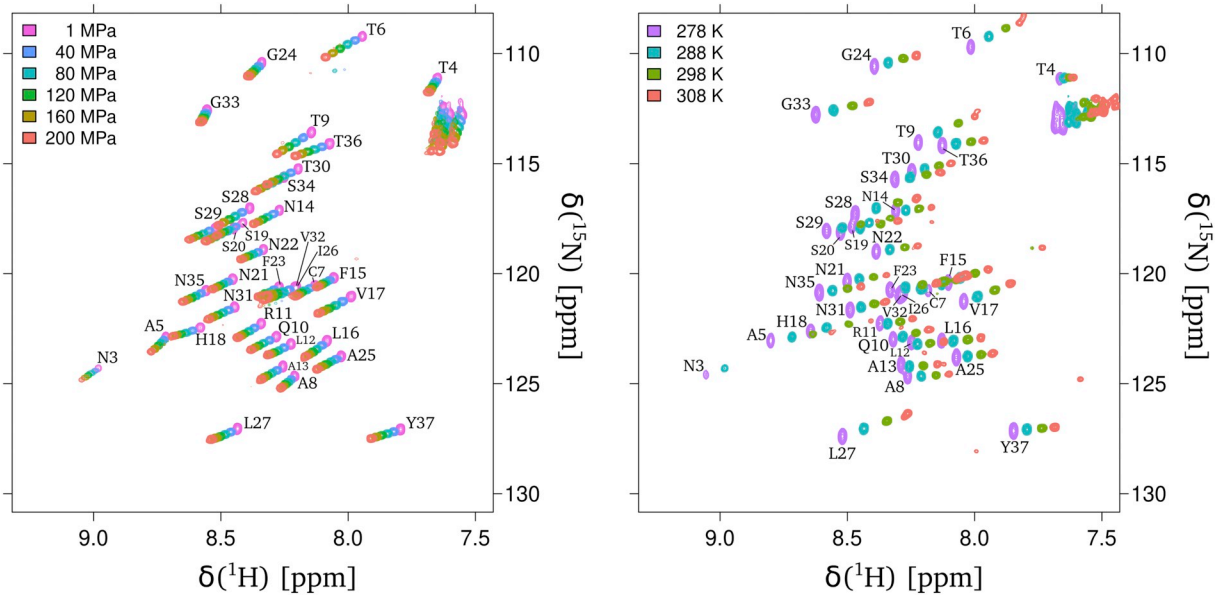

Fig. 1. Amide proton and nitrogen shift changes induced by pressure and temperature. [^{1}H-^{15}N] HSQC spectrum recorded at 800 MHz proton frequency. (left) Spectrum at 288 K and pressures from 1 MPa to 200 MPa in steps of 40 MPa. (right) Spectrum at 1 MPa and temperatures from 278 K to 308 K in steps of 10 K. The sample contained 110 µM ^{15}N-enriched hIAPP(1–37) in 10 mM Na-acetate buffer, pH 5.5, 0.1 mM DSS in 90% ^1H_2O / 10% ^2H_2O.

signal intensities are shown as semi-transparent lines and the mean value as a bold line. At 278 K, already at 20 MPa a moderate decrease of the average signal intensity to 95% of the initial intensity was observed, but remains constant up to a pressure of 200 MPa. For 288 K, the intensities remain constant up to approx. 140 MPa and show a minimal decrease to approx. 95% of the initial intensity for pressures above 140 MPa.

Both temperatures 278 K and 288 K show almost no influence of the pressure on the signal intensity. Only the deviations from the mean value are larger at 288 K, while at 278 K after a first drop the signal intensity over the total pressure range is nearly constant. To assess the influence of the change in the exchange rates of the amide protons with temperature, the individual line widths were also analyzed as a function of pressure. The line widths increase approximately 1 Hz at 200 MPa compared to ambient conditions, but generally display large fluctuations over the measured pressure range, in particular the line widths of the amide protons. Therefore, a large impact of the exchange rates on the signal intensities seems unlikely. At higher temperatures, a significant influence of the pressure on the signal intensities can be observed. At 298 K, the intensities remain nearly constant until about 60 MPa, while for pressures above 60 MPa a linear decrease of the signal intensities to approx. 75% of the initial intensity was observed. This behavior is reflected in both the individual intensities and the mean value of the signal intensities. The observed signal intensities at 308 K showed a linear decrease with pressure to a value of approx. 60% at 200 MPa. Again, the behavior of the mean value is reflected in the individual measurements. The resulting signal reduction indicates formation of large aggregates.

After each pressure series (3 MPa–200 MPa), the reversibility after pressure application was checked and a second measurement was recorded at 3 MPa. At 278 K and 288 K, the intensities were almost identical to those observed at the beginning. Since an increase in pressure led to almost no decrease in the signal intensity, good reversibility was to be expected. At 298 K and 308 K, a strong decrease in intensity with pressure was observed (Fig. 2). The release of pressure back to 3 MPa did not result in a full recovery of the signal intensities and the initial signal intensities at 3 MPa were only partially recovered (in the order of 60%). The time distance between the measurements at 200 MPa and the reversibility measurement at 3 MPa was approx. 30 min. Within 30 min, the signal intensities at temperatures 298 K and 308 K did not recover. However, slow de-polymerization of the aggregates (or fibrillar structures) cannot be ruled out.

Summing up, we can state that higher temperatures usually lead to the disappearance of NMR signals in hIAPP (Fig. 2). Only at 278 K and 288 K, the intensities of the NMR signals displayed nearly constant behavior with increasing pressure and time, since the concentration range of 110 μM is well below the critical aggregation concentration at these temperatures.

Most of the amide resonances shift continuously with pressure and temperature, the majority of resonances to lower fields. The obtained pressure induced chemical shift changes are completely reversible. For a quantitative phenomenological description of the pressure induced ^{1}H and ^{15}N shift changes, the chemical shifts were first corrected for unspecific random-coil effects.[34] The resulting ^{1}H and ^{15}N chemical shift data were fitted with a second order Taylor expansion (Eq. (1)). The linear pressure coefficient B_1 and the non-linear pressure coefficient B_2 for the amide proton and the amide-templated peptide backbone were determined. The pressure coefficients for the amide proton are shown in Fig. 3. The result for the linear pressure coefficient B_1 over the sequence is a mean value of 0.08 ppm/GPa (278 K), 0.07 ppm/GPa (288 K), 0.10 ppm/GPa (293 K) and 0.09 ppm/GPa at 308 K. The standard deviation for all temperatures is approx. 0.18 ppm/GPa. Averaged over all temperatures, H18 shows the largest positive value with 0.43 ppm/GPa and T4 the largest negative value with −0.53 ppm/GPa. For the non-linear pressure coefficient B_2, we obtain an average value of −0.34 ppm/GPa^2 (278 K), −0.28 ppm/GPa^2 (288 K), −0.32 ppm/GPa^2 (298 K) and − 0.23 ppm/GPa^2 at 308 K. The standard deviation for all temperatures is approx. 0.50 ppm/GPa^2. The largest positive value showed A5 with 0.56 ppm/GPa^2, the largest negative value H18 with −1.32 ppm/GPa^2.

The pressure dependence of the amide nitrogen for the peptide backbone is shown in Fig. 4. The result for the first order pressure coefficient B_1 is a value averaged over the sequence of 1.12 ppm/GPa (278 K), 0.88 ppm/GPa (288 K), 0.97 ppm/GPa (298 K) and 1.09 ppm/GPa at 308 K. The standard deviation for the different temperatures is approx. 1.00 ppm/GPa. The largest positive averaging over all temperatures is found for V17 with 3.55 ppm/GPa, the largest negative value for Y37 with −0.84 ppm/GPa. Averaged over the sequence we obtained for the non-linear pressure coefficient B_2 a value of −4.14 ppm/GPa^2 (278 K), −2.97 ppm/GPa^2 (288 K), −2.81 ppm/GPa^2 (298 K) and − 2.67 ppm/GPa^2 for 308 K. For the temperatures 288 K to 308 K the standard deviation is around 2.70 ppm/GPa^2, at 278 K with 4.39 ppm/GPa^2 it is significantly higher. Averaged over temperature, the highest positive value was found for T6 with 4.05 ppm/GPa^2, the largest negative value for V17 is −8.34 ppm/GPa^2.

As already shown for the pressure behavior of tetrapeptides[39,40], the linear pressure coefficient B_1 is almost mirror-inverted to the non-linear coefficient B_2. This can be seen in Fig. 5, which shows the correlation between the pressure coefficients for the two nuclei ^{15}N and $^{1}H^{N}$. There is a strong negative correlation of $r(H^N) = -0.84$ and $r(N) = -0.70$ for both atoms.

The analysis of the [^{1}H-^{15}N] HSQC spectra provides information on the pressure behavior of the nitrogen nuclei and protons. These are in close spatial proximity, but have different chemical behavior (e.g., chemical exchange, solvent interaction). Therefore, a comparison of the pressure coefficients for the nitrogen nucleus and the protons seems to be interesting (Fig. 6). The pressure coefficients were calculated from chemical shifts weighted as described by Schumann et al. [35].

For the linear pressure coefficient B_1 we found the largest deviations between the nuclei at the beginning of the sequence, especially for T4. The largest part of the differences is positive. Compared to the environment, L16 also shows a big difference followed by a change of sign at H18. From H18, only small differences between the nuclei are seen. Based on the absolute values, B_1 yields an average difference of 0.20 ppm/GPa.

The majority of the differences for the non-linear pressure coefficient B_2 are negative and mirror the behavior of B_1. This is particularly evident at the positions V32, H18 and Q10, since in all cases the sign is opposite to the rest of the sequence. Large differences can again be found at the beginning of the sequence for N3 as well as for A8, H18 and the cluster from I26 to S28. Relative to the absolute values, there is an average deviation of 0.44 ppm/GPa^2 for the non-linear pressure coefficient B_2.

Correlation of the weighted nuclei for the two pressure coefficients B_1 and B_2 yielded Pearson correlation coefficients of $r(B_1) = 0.47$ and $r(B_2) = 0.86$. The low correlation coefficient for the linear pressure coefficient B_1 can be attributed to the strong differences at the beginning of the sequence between N3 and T9 (compare Figs. 3 and 4), while for the non-linear pressure coefficient B_2 the difference is larger but the correlation is higher (offset).

For a more compact representation, the obtained first- and second-order pressure coefficients B_1 and B_2 for the two nuclei were combined using amino specific weighting factors [35] and plotted in Fig. 7 as a function of the sequence position for the four different temperatures. Only a few amide resonances could not be observed with sufficient intensity, the amide groups of K1, C2, and N3, which was only observable at 288 K and 278 K. The pressure coefficients of the combined chemical shift tend to behave very similar to the pressure coefficients of the individual nuclei already shown ($^{1}H^{N}$: Fig. 3 ^{15}N: Fig. 4). It is noticeable that in most cases a positive linear coefficient B_1 is correlated with a negative non-linear coefficient B_2. Exceptions are the amino acids N3 to A5, F15, G33 and Y37. Here, the pressure coefficients are

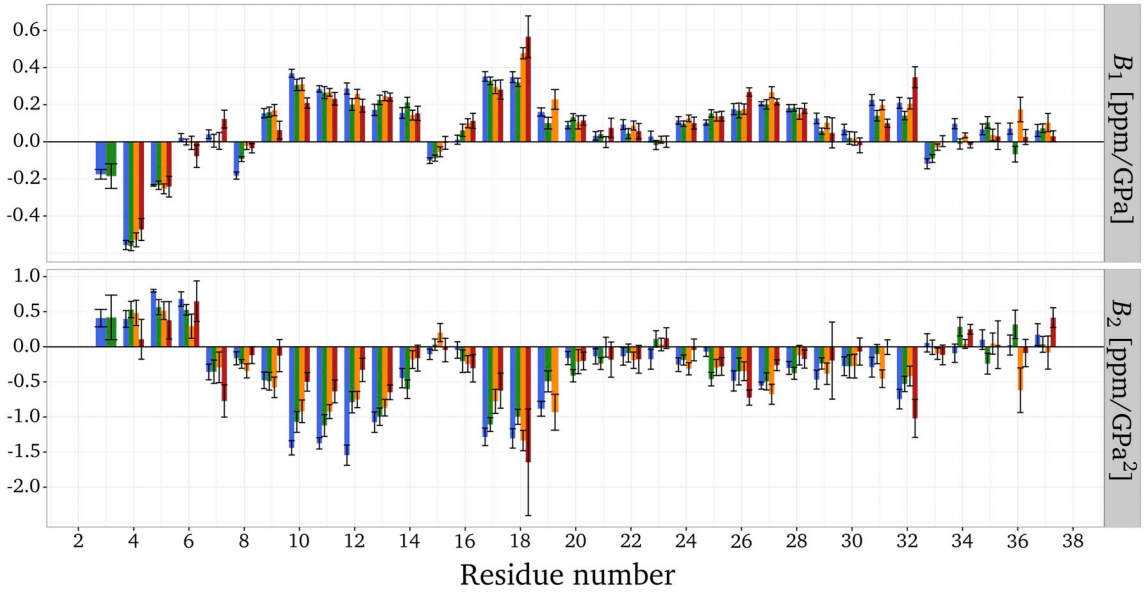

Fig. 3. Plot of the first and second order pressure coefficients of $^1H^N$ of hIAPP(1–37). The sample contained 110 μM ^{15}N-enriched hIAPP(1–37) in 10 mM Na-acetate buffer, pH 5.5, 0.1 mM DSS in 90% ^1H_2O/10% ^2H_2O. The first and second order pressure coefficients of $^1H^N$ were calculated from the [^{1}H-^{15}N] HSQC spectra recorded at different pressures in pressure steps of 20 MPa up to 200 MPa. Temperatures: 278 K (blue), 288 K (green), 298 K (orange), and 308 K (red). The Taylor coefficients were corrected for random-coil effects (see Materials and Methods). (Top) First-order pressure coefficients, B_1. (Bottom) Second-order pressure coefficients, B_2. Figure based on Beck Erlach et al.[38]. (For interpretation of the references to colour in this figure legend, the reader is referred to the web version of this article.)

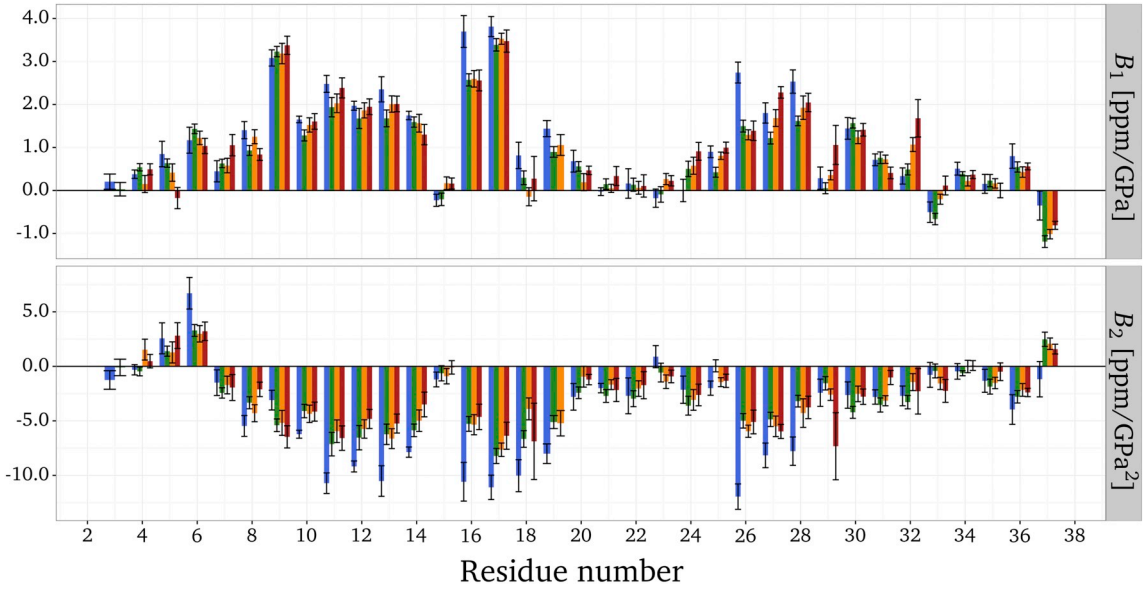

Fig. 4. Plot of the first and second order pressure coefficients of ^{15}N of hIAPP(1–37). The sample contained 110 μM ^{15}N-enriched hIAPP(1–37) in 10 mM Na-acetate buffer, pH 5.5, 0.1 mM DSS in 90% ^1H_2O/10% ^2H_2O. The first and second order pressure coefficients of ^{15}N were calculated from the [^{1}H-^{15}N] HSQC spectra recorded at different pressures in pressure steps of 20 MPa up to 200 MPa. Temperatures: 278 K (blue), 288 K (green), 298 K (orange), and 308 K (red). The Taylor coefficients were corrected for random-coil effects (see Materials and Methods). (Top) First-order pressure coefficients, B_1. (Bottom) Second-order pressure coefficients, B_2. Figure based on Beck Erlach et al.[38]. (For interpretation of the references to colour in this figure legend, the reader is referred to the web version of this article.)

opposite to the rest of the pattern. It is remarkable that the amino acids F15 and the area around F23 exhibit almost no or a very weak pressure dependence of the chemical shift.

Looking close into the data one can recognize distinctive patterns in the amino acid sequence of the combined pressure coefficients (Fig. 7). Interestingly, from the first N-terminal amino acids, which are characterized by the disulfide bridge between C2 and C7 and form a hook-like structure, N3, T4, A5 display negative B_1 values and positive B_2 values. Starting with T9, a block of amino acids ranging to N14 displayed large positive B_1 values and negative B_2 values for the chemical shifts. F15 showed only a very weak pressure sensitivity with very small B_1 as well as B_2 values close to zero for the chemical shifts (Fig. 7). Subsequently, a block of amino acids ranging from L16 to N22 displayed positive B_1 and negative B_2 values. Here, V17 exhibits the largest positive B_1 values and negative B_2 values while the other residues S20, N21, and N22 displayed only moderate and weak positive B_1 values and negative B_2 values. F23, the second phenylalanine in the hIAPP (1–37) sequence, showed again a very weak pressure sensitivity, represented by very small B_1 and B_2 values close to zero (Fig. 7). The next block of amino acid residues with positive B_1 and negative B_2 values for

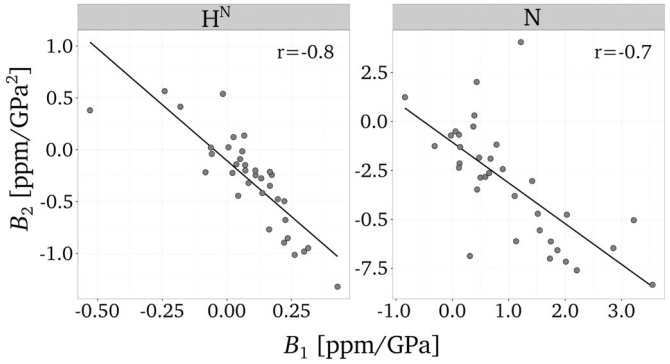

Fig. 5. Correlation of the first- and second-order pressure coefficients of ^{15}N and $^{1}H^{N}$ of hIAPP(1–37). The sample contained 110 μM ^{15}N-enriched human IAPP(1–37) in 10 mM Na-acetate buffer, pH 5.5, 0.1 mM DSS in 90% $^{1}H_2O$/10% $^{2}H_2O$. The first- and second-order pressure coefficients of ^{15}N and $^{1}H^{N}$ were calculated from the [^{1}H-^{15}N] HSQC spectra recorded at different pressures in pressure steps of 20 MPa up to 200 MPa. The Taylor coefficients were corrected for random-coil effects and averaged over temperatures (see Materials and Methods). Pearson correlation coefficients were determined to $r(^{1}H^{N}) = -0.8$ and $r(^{15}N) = -0.70$. The average B_2/B_1 ratio is −3.1 1/GPa for $^{1}H^{N}$ and − 3.5 1/ GPa for ^{15}N.

the chemical shifts ranges from G24 to V32. However, a dip in the values of the combined pressure coefficients B_1 and B_2 could be observed for amino acid S29 (Fig. 7). The combined pressure coefficients B_1 and B_2 of the last 5 C-terminal residues G33, S34, N35, T36, and Y37 were all very small, indicating very low pressure sensitivity for these C-terminal residues.

Also of interest is the change in pressure coefficients with respect to the predecessor in the sequence which could indicate areas in the peptide sequence connected to the strongest sensitivity for pressure. In Fig. 8, the differences of the pressure coefficients of the predecessor are shown depending on the amino acid sequence. The mean difference over the sequence for B_1 is 0.005 ppm/GPa and 0.0006 ppm/GPa^2 for B_2. This indicates that the changes in pressure coefficients across the sequence are almost completely eliminated.

In Fig. 8, the standard deviation is also shown as a dashed line. For B_1 it is −0.38 ppm/GPa and 1.05 ppm/GPa^2 for B_2. The linear pressure coefficient B_1 for the amino acids N3, T4, A5, T9, F15, L16, V17, H18, S29 and G33 were found outside the standard deviation. For the non-linear pressure coefficient, the residues C7, Q10, N14, F15, L16, V17, S20, I26, G33 and Y37 were outside of the standard deviation.

The pressure series for the hIAPP was recorded at temperatures 278 K, 288 K, 298 K and 308 K. The derived pressure coefficients for these temperatures are shown in Figs. 3, 4 and 7. It is noteworthy that some of the derived pressure coefficients display a strong temperature dependence while others display almost no influence on temperature. Hence, the temperature dependence was checked using a linear model with pressure coefficients of the combined chemical shifts (Fig. 7). The temperature dependence of the two combined pressure coefficients B_1 and B_2 is depicted in Fig. 9.

For the linear pressure coefficient B_1, the mean value of the temperature dependence is $3{\cdot}10^{-5}$ ppm/(GPa·K) with a standard deviation of 0.006 ppm/(GPa·K). Outliers with more than one standard deviation relative to the mean could be found at residues A5, C7, Q10, F15, H18, G24, L27 and the sequence area from N31 to S34. The mean value of the temperature dependence for the non-linear pressure coefficient B_2 is 0.02 ppm/(GPa^2·K) with a standard deviation of 0.03 ppm/(GPa^2·K). Outliers with more than one standard deviation relative to the mean are observed for the areas of A5 to C7, Q10 to N14, V17, I26 to S29 and G33.

3.2. Temperature dependence of the chemical shifts of hIAPP

In the previous chapter, the pressure dependence of the amide group of the IAPP peptide backbone was investigated. Similarly, the influence of temperature on the chemical shifts of the amide group of the peptide backbone for IAPP can be investigated. In contrast to the 11 measuring points for the investigation of the pressure effects, only 4 measuring points were available for the examination of the temperature. Therefore, in contrast to the evaluation of the pressure effects (second-degree polynomial), the data were fitted with a linear model (see Materials and Methods). The linear temperature coefficients C_1 over the sequence of IAPP for the nuclei H^{N} and N are displayed in Fig. 10. The data revealed clearly negative temperature coefficients C_1. For H^{N}, a mean value of −6.0 ppb/K with a standard deviation of 1.5

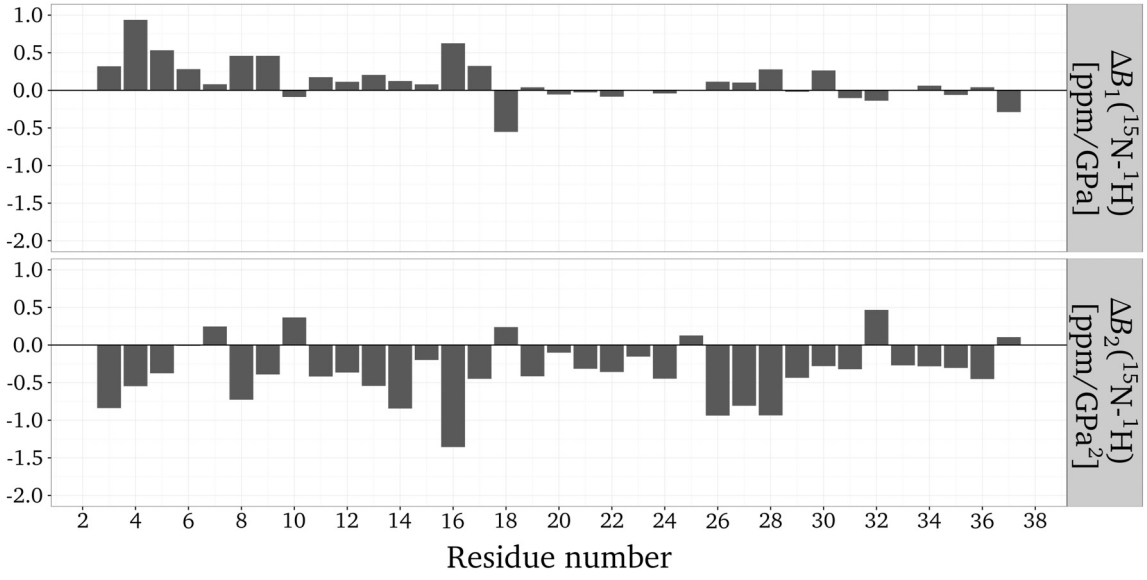

Fig. 6. Difference between the pressure coefficients of the amide nitrogen and the amide protons in hIAPP. The sample contained 110 μM ^{15}N-enriched hIAPP(1–37) in 10 mM Na-acetate buffer, pH 5.5, 0.1 mM DSS in 90% $^{1}H_2O$/10% $^{2}H_2O$. The first and second order pressure coefficients of ^{15}N and $^{1}H^{N}$ were calculated from the [^{1}H-^{15}N] HSQC spectra recorded at different pressures in pressure steps of 20 MPa up to 200 MPa. The Taylor coefficients were corrected for random-coil effects and averaged over temperatures (see Materials and Methods). Pearson correlation coefficients were determined to $r(B_1) = 0.47$ and $r(B_2) = 0.86$. The mean deviation for the nuclei is 0.2 ppm/GPa for B_1 and 0.44 ppm/GPa^2 for B_2.

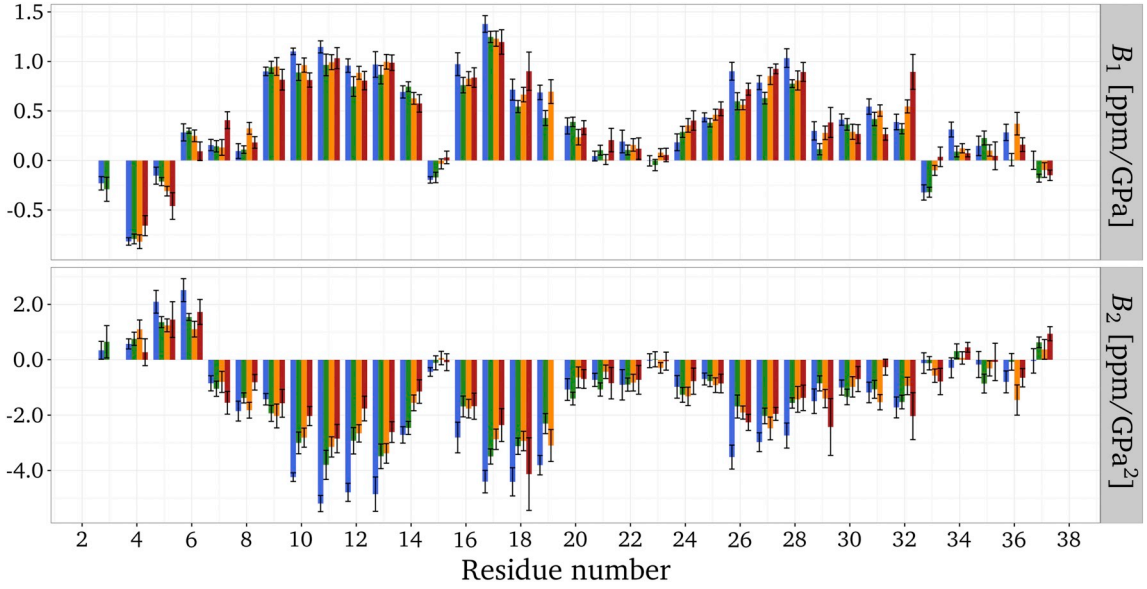

Fig. 7. Plot of the combined first and second order pressure coefficients of hIAPP(1–37). The sample contained 110 μM ^{15}N-enriched hIAPP(1–37) in 10 mM Na-acetate buffer, pH 5.5, 0.1 mM DSS in 90% ^1H_2O/10% ^2H_2O. The combined first and second order pressure coefficients were calculated from the [^{1}H-^{15}N] HSQC spectra recorded at different pressures in pressure steps of 20 MPa up to 200 MPa. Temperatures: 278 K (blue), 288 K (green), 298 K (orange), and 308 K (red). The Taylor coefficients were corrected for random-coil effects (see Materials and Methods). (Top) Combined first order pressure coefficients, B_1. (Bottom) Combined second order pressure coefficients, B_2. Figure based on Beck Erlach et al. [38]. (For interpretation of the references to colour in this figure legend, the reader is referred to the web version of this article.)

ppb/K were observed. Relative to the mean value for H^N, the residues T4, A5, T9, R11 to A13, S20, I26 to S28 and V32 showed deviations larger than one standard deviation. For the amide nitrogen, a mean value of −14.7 ppb/K with a standard deviation of 10.23 ppb/K was obtained. Large deviations were found for residues N3, T4, T6, A8, T9, L12 to N14, V14 and I26 to L27.

An exceptionally small temperature coefficient for both nuclei was found for the residue T4, while T9 displayed a strong temperature dependence together with the sequence areas H18–S20 and I26–S28. The Pearson correlation coefficient of the nuclei H^N and N is $r = 0.74$.

The temperature coefficients have been additionally corrected for the intrinsic temperature effect of the respective amino acid according to Kjaergaard et al. [36] and are shown in Fig. 11. While there are no major changes in the temperature dependence of the nitrogen nuclei after the random-coil based correction, the proton temperature coefficients exhibit significant changes and turn positive in majority. Thus, the mean value for H^N is now positive with 1.7 ppb/K and a standard deviation of 1.6 ppb/K. Relative to the mean value, the amino acid residues N3, T4, A8, T9, L12, A13, S20, G24 to S28 and V32 showed deviations larger than one standard deviation. For the amide nitrogen

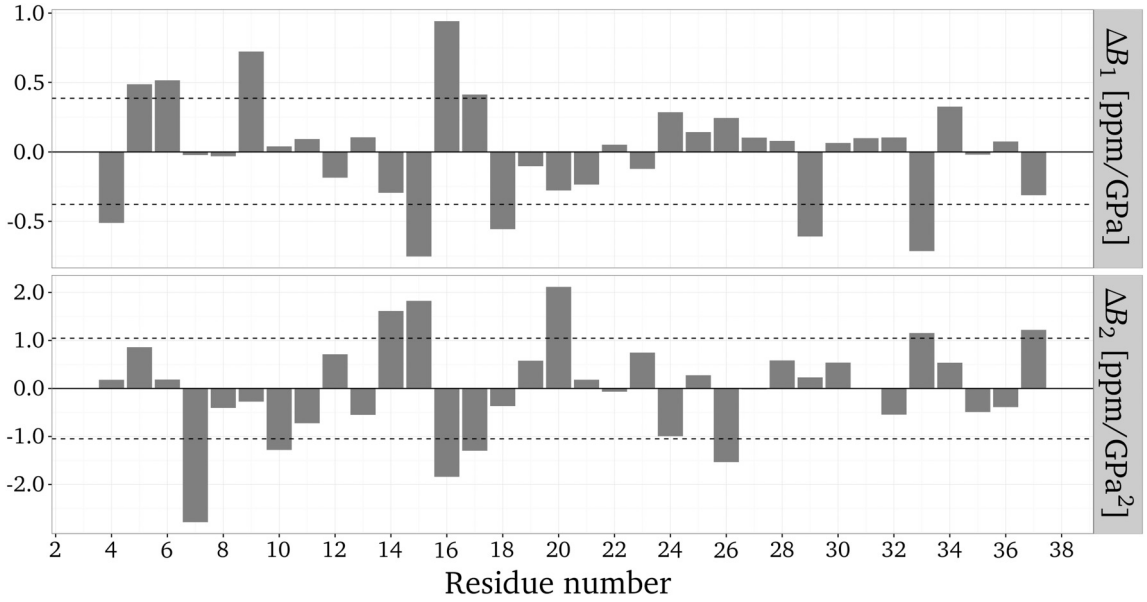

Fig. 8. Plot of the difference of the combined first and second order pressure coefficients B_1 and B_2 to the preceding sequential amide group of hIAPP(1–37). The sample contained 110 μM ^{15}N-enriched hIAPP(1–37) in 10 mM Na-acetate buffer, pH 5.5, 0.1 mM DSS in 90% ^1H_2O/10% ^2H_2O. The combined first- and second-order pressure coefficients were calculated from the [^{1}H-^{15}N] HSQC spectra recorded at different pressures in pressure steps of 20 MPa up to 200 MPa. The Taylor coefficients were corrected for random-coil effects (see Materials and Methods). The pressure coefficients are averaged over all temperatures. One standard deviation relative to the mean is indicated by the dashed line.

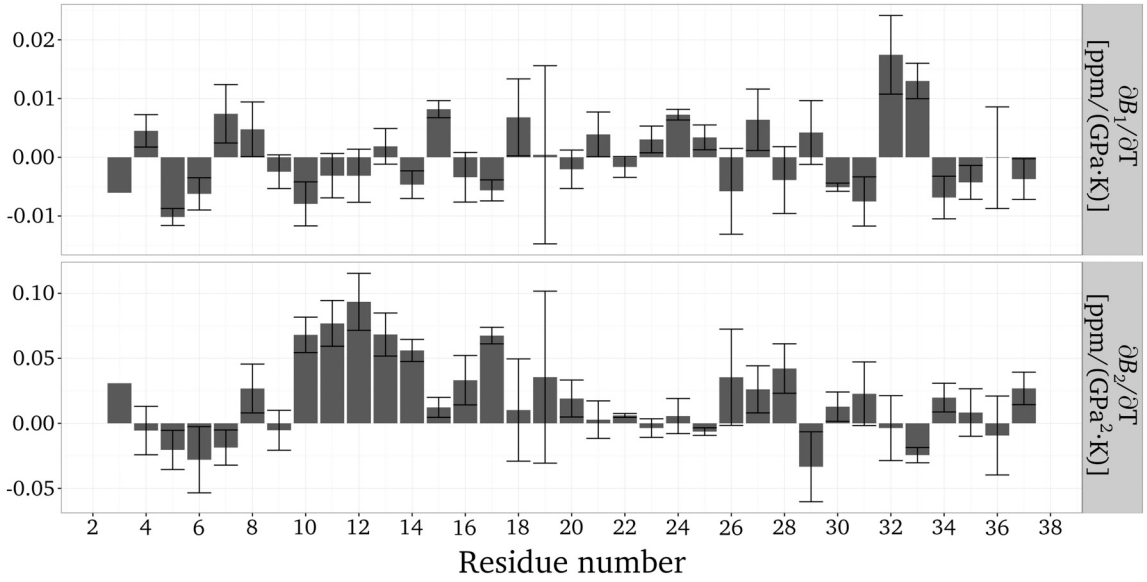

Fig. 9. Plot of the linear temperature dependence of the combined first- and second-order pressure coefficients, B_1 and B_2, of hIAPP(1–37). The sample contained 110 μM ^{15}N-enriched hIAPP(1–37) in 10 mM Na-acetate buffer, pH 5.5, 0.1 mM DSS in 90% $^{1}H_2O$/10% $^{2}H_2O$. The combined first- and second-order pressure coefficients were calculated from the [^{1}H-^{15}N] HSQC spectra recorded at different pressures in pressure steps of 20 MPa up to 200 MPa. The Taylor coefficients were corrected for random-coil effects (see Materials and Methods).

atoms, a mean value of −8.8 ppb/K with a standard deviation of 10.1 ppb/K was observed. The amino acid residues N3, T4, T6, A8, T9, L12, A13, L27, S28 and Y37 showed deviations larger than one standard deviation. The corrected temperature coefficients of the nuclei H^N and N showed a slightly higher Pearson correlation coefficient of $r = 0.78$ compared to the uncorrected temperature coefficients.

3.3. Correlation analysis of pressure and temperature dependence of chemical shifts of hIAPP

The knowledge of the pressure and temperature dependence of the amide groups of the peptide backbone for hIAPP allows to perfom a correlation analysis between the coefficients. For the analysis the random-coil corrected coefficients were used, temperature coefficient C_1 was corrected according to Kjaergaard et al. [36] and pressure coefficients B_1 and B_2 according to Koehler et al. [34] The results are shown and summarized in Fig. 12. Fig. 12a) depicts the correlations between C_1^{corr} and B_1 and B_2 for the nuclei H^N (green) and N (blue), respectively. In both cases, the nitrogen nuclei displayed a larger variance of the data. The correlation values between the coefficients are shown in Fig. 12b), where the typical strong correlations between B_1 and B_2 with $r(H^N) = -0.84$ and $r(N) = -0.70$ and a strong correlation between the non-linear pressure coefficients of the nuclei H^N and N with $r(N) = 0.85$ could be observed. In addition, the linear pressure coefficient $B_1(H^N)$ correlates with $B_2(N)$ with a correlation coefficient of $r = -0.69$. There is a strong correlation between the temperature

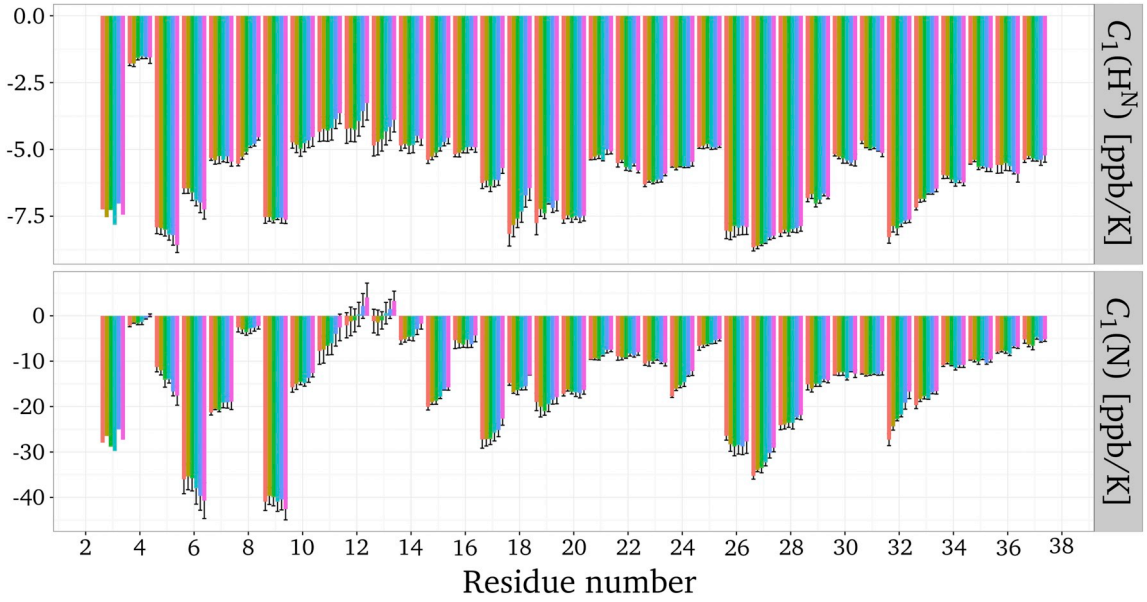

Fig. 10. Plot of the linear temperature coefficient C_1 for H^N (top) and N (bottom) of hIAPP(1–37). Indicated are the different pressure steps of 40 MPa from 1 MPa (red) to 200 MPa (pink) with Pearson correlation coefficient of $r = 0.74$. The sample contained 110 μM ^{15}N-enriched hIAPP(1–37) in 10 mM Na-acetate buffer, pH 5.5, 0.1 mM DSS in 90% $^{1}H_2O$/10% $^{2}H_2O$. (For interpretation of the references to colour in this figure legend, the reader is referred to the web version of this article.)

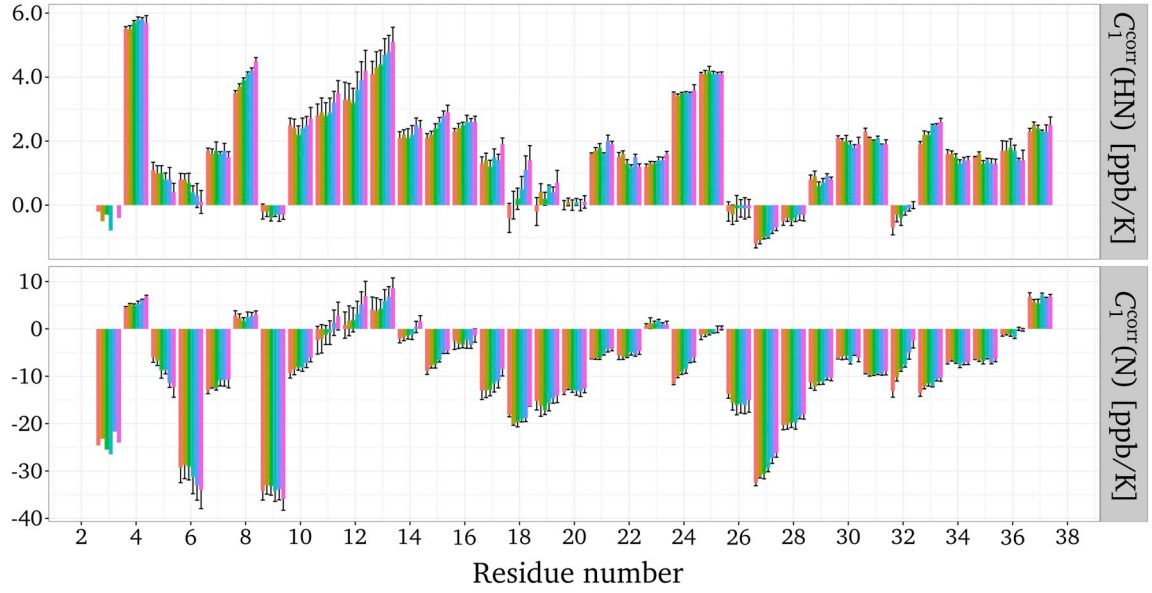

Fig. 11. Plot of the corrected linear temperature coefficient C_1^{corr} for H^N (top) and N (bottom) of hIAPP(1–37). Indicated are the different pressure steps of 40 MPa from 1 MPa (red) to 200 MPa (pink) with a Pearson correlation coefficient of $r = 0.78$. The sample contained 110 μM ^{15}N-enriched hIAPP(1–37) in 10 mM Na-acetate buffer, pH 5.5, 0.1 mM DSS in 90% ^1H_2O/10% ^2H_2O. The temperature coefficients were corrected for random-coil effects (see Materials and Methods). (For interpretation of the references to colour in this figure legend, the reader is referred to the web version of this article.)

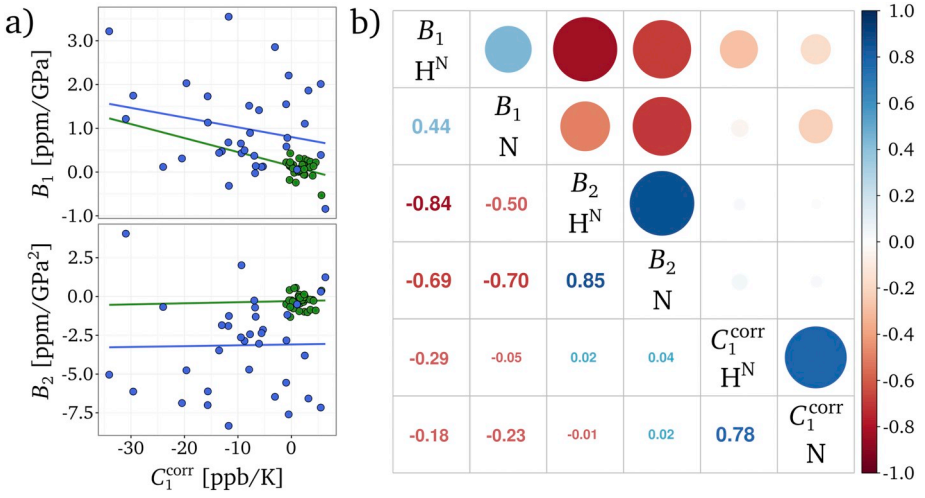

Fig. 12. Correlation analysis between the linear temperature coefficient C_1^{corr} and the combined first and second order pressure coefficients B_1 and B_2 of hIAPP(1–37). (a) Correlations for H^N (green) and N (blue) between the linear temperature coefficient C_1^{corr} and the combined first and second order pressure coefficients B_1 and B_2 of hIAPP(1–37). (b) Correlation table for the different coefficients and nuclei. The sample contained 110 μM ^{15}N-enriched hIAPP(1–37) in 10 mM Na-acetate buffer, pH 5.5, 0.1 mM DSS in 90% ^1H_2O/10% ^2H_2O. All coefficients were corrected for random-coil effects (see Materials and Methods). (For interpretation of the references to colour in this figure legend, the reader is referred to the web version of this article.)

coefficients C_1^{corr} of the nuclei H^N and N with $r = 0.78$. The correlation between the temperature and the linear pressure coefficients is rather weak with values of $r(H^N) = -0.29$ and $r(N) = -0.23$, respectively.

Figs. 10 and 11 show a significant dependence of the corrected temperature coefficient C_1^{corr} on the applied pressure for many amino acids. Due to this observation we investigated the pressure dependence of the corrected temperature coefficient C_1^{corr} using a linear model (see Materials and Methods). The majority of the coefficients $\partial C_1^{corr}/\partial p$ determined are positive, indicating an increase in the temperature sensitivity with increasing pressure. The amino acids A5 and T6 display a significant decrease in the temperature dependence for both nuclei with pressure. The largest pressure influence on the temperature coefficients is found for the proton at H18 and for the nitrogen atom at V32. The amide protons displayed a mean value of 1.16 ppb/(GPa·K) and for the amide nitrogen a mean value of 8.77 ppb/(GPa·K) was found with according standard deviations of 2.59 ppb/(GPa·K) for the protons and 15.49 ppb/(GPa·K) for the nitrogen atoms. For the protons the amino acid residues A5, T6, A8, L12, A13, F15, H18, N31 and S34 to T36 exhibit values above one standard deviation. For the nitrogen atoms, the amino acid residues A5, T6, T9, R11, L12, G24, L27, and V32 displayed the largest deviations from the mean value.

The temperature dependence of the pressure coefficients B_1 and B_2 can be compared with the pressure dependence of the temperature coefficient C_1^{corr} on the sequence of IAPP, leading to a strong negative correlation of $r = -0.61$ between the temperature dependencies of both pressure coefficients B_1 to B_2 for the nuclei H^N and N (Fig. 14b). In addition, $\partial C_1^{corr}/\partial p$ displayed a strong correlation between the nuclei of $r = 0.64$. Between $\partial C_1^{corr}/\partial p$ and the temperature dependence of the linear pressure coefficient B_1 a correlation coefficient of $r = 0.64$ could be found while for $\partial C_1^{corr}/\partial p$ and $\partial B_2/\partial T$ the correlation coefficient is $r = 0.56$.

The correlation analyses of the coefficients (see Figs. 12 and 14) generally revealed a greater variance for the amide nitrogen (blue) compared to the amide protons (green). This holds true for both, the correlations between the temperature (C_1^{corr}) and pressure coefficients (B_1 and B_2) themselves as well as for the pressure dependence of the temperature coefficients $\partial C_1^{corr}/\partial p$ and the temperature dependence of the pressure coefficients $\partial B_1/\partial T$ and $\partial B_2/\partial T$ (Fig. 14a). In addition, it appears that the correlation between $\partial C_1^{corr}/\partial p$ and $\partial B_1/\partial T$ for the two nuclei of the amide group is almost identical.

4. Discussion

Considering the intensities at the signal maxima of hIAPP for the different temperatures and pressures (Fig. 2), a constant behavior of the intensities over the pressure is found only for the temperatures 278 K and 288 K, while for the temperatures 298 K and 308 K a decrease of the intensities has been noted. The aggregation propensity of hIAPP is influenced by higher temperatures and the application of high pressure cannot inhibit the aggregation at 298 K and 308 K. This is also indicated by the reversibility measurements carried out, since releasing the pressure after pressure application back to 3 MPa did not lead to a full recovery of the signal intensities. Comparing the behavior of the signal intensities of hIAPP with the pressure-induced depolymerization of the amyloid-β [41], it seems apparent that hIAPP exists completely in its monomeric form in solution in the temperature range from 278 K to 288 K. This is in clear contrast to the amyloid-β peptide, where a signal increase can be observed by increasing pressure [41], while in the case of hIAPP no major changes in signal intensities with time or pressure are observed at these low temperatures.

Considering the pressure dependence of hIAPP, we noticed that especially the amino acid residues F15 and F23 exhibit almost no pressure sensitivity, independent of temperature. Since the pressure response was corrected for intrinsic random-coil effects, the two phenylalanines display the same behavior as in the random-coil peptide Ac-Gly-Gly-Phe-Gly-NH_2. A better classification of these effects can be achieved when considering the point mutations of hIAPP [42,43]. It has been shown that single mutations can attenuate, enhance or completely prevent the aggregation of IAPP. Single point mutations abolishing the amyloid formation of hIAPP are located either in the region of amino acid residues 12–17 and at residue 21 as well as in the region encompassing residues 24–28 [43]. Apart from the amino acid residues F15 and N21, these areas display an increased pressure sensitivity. An increase in aggregation propensity was found for point mutations at sites F15, V17, and S20 [43]. Here, F15 shows almost no pressure sensitivity, S20 displays a medium and V17 a strong pressure sensitivity. A reduction in amyloid formation is found for mutations of the amino acids A13, F15, S20, F23, A25, N31, N35 and Y37 [43]. These are mainly at the C-terminal end of the peptide sequence. Considering the pressure dependence of these residues, there is almost no pressure effect for the phenylalanines and only moderate pressure effects for the residues S20, A25 and N31, whereas the majority of amino acid residues at the end of the sequence display only minor pressure effects.

Interestingly, depending on the mutation, point mutations at the amino acids F15 and S20 led to a strengthening or weakening of the aggregation [44,45]. According to Tu and Raleigh [44], the aromatic amino acids F15, F23 and Y37 show a particularly strong influence on the aggregation. The mutation F15L leads to an aggregation behavior twice as high as of the wild type, while the F23L mutation reduces the aggregation propensity by 50% and Y37L by 66%. For the position F15 it has also been shown that an exchange to leucine, norleucine, isoleucine and tert-leucine shows a correlation of the aggregation sensitivity to the α-helical propensity of the amino acid sequence [44]. This behavior is consistent with the observations from other groups, where the onset of aggregation is characterized by the formation of helical structures in the sequence region around amino acid positions 8–22 [45–47]. Similar studies for the amyloid-β show a different behavior at positions 19 and 20 compared to hIAPP [38,48]. Substitutions that increase the propensity for β-sheet formation result in increased aggregation, and a decrease in β-sheet propensity leads to decreased aggregation [49].

Since the pressure effects of the chemical shift were recorded at different temperatures, the influence of the temperature on the pressure coefficients B_1 and B_2 was investigated as well (Fig. 9). The pressure coefficients were determined from the pressure dependence of the combined chemical shift [35]. It was found that the non-linear pressure coefficient B_2 with an average temperature dependence of 0.02 ppm/(GPa^2·K) exhibits a significantly higher temperature dependence than the linear pressure coefficient B_1 with an average temperature dependence of $3{\cdot}10^{-5}$ ppm/(GPa·K). In case of B_1, a strong temperature dependence was seen for the amino acid residues V32 and G33. In addition, the amino acid sequence of Q10 to N14 is particularly noticeable for the temperature dependence of B_2. These areas also show a distinctive behavior regarding the pressure dependence. Thus, for B_1 sequential to amino acid V32 a strong drop in the pressure dependence (Fig. 8) and for B_2 in the sequence range Q10 to N14 strong pressure effects (Fig. 7) were observed. The accuracy of the measurement range revealed areas in which the temperature dependence of the pressure coefficients shows similarities with the strength of the pressure effect.

Furthermore, the temperature dependence of the chemical shift of the amide group nuclei of the peptide backbone of hIAPP was investigated. The intrinsic temperature effects of the respective amino acids were corrected according to Kjaergaard et al. [36]. The mean temperature coefficient for the amide protons changed from 6 ppb/K (without correction) to 1.7 ppb/K (with correction). For the nitrogen nuclei, we observed a change from −14.7 ppb/K (without correction) to −8.8 ppb/K. In both cases, the nitrogen nuclei showed a significantly larger temperature dependence. After correction, vanishing temperature coefficients are found for some amino acids (N3, T9, S20, I26, and V32). It was shown by Baxter and Williamson [50] that slowly exchanging amide protons with a temperature coefficient > −4.5 ppb/K participate in a hydrogen bond, while temperature coefficients < −4.5 ppb/K indicate no involvement in a hydrogen bond. However, this refers to temperature coefficients which have not been corrected for the intrinsic temperature effect of the respective amino acids. Looking at the uncorrected temperature coefficients (Fig. 10), only T4 exhibits a temperature coefficient that indicates the participation in a hydrogen bond.

Analogous to the temperature dependence of the pressure coefficients, the pressure dependence of the temperature coefficients was investigated. Especially the amino acids A5 and T6 with clearly negative $\partial {C_1}^{corr}/\partial p$, the range from Q10 to F15 and the amino acids V32 and G33 with clearly positive $\partial {C_1}^{corr}/\partial p$ are attracting attention (Fig. 13). Since the already described coefficients and their pressure and temperature dependence have similar patterns depending on the sequence, correlations between them were determined. Strong Pearson correlation coefficients were found between the pressure coefficients B_1 and B_2 with −0.84 (H^N) and − 0.7 (N) but also between the nuclei H^N and N with 0.85 (B_2) and 0.78 (${C_1}^{corr}$) and between different nuclei and pressure coefficients with $r(B_2(N)\text{-}B_1(H^N)) = -0.69$. Looking at the correlations of the pressure and temperature dependencies of the coefficients, strong correlations were found between the temperature dependencies of the pressure coefficients $\partial B_1/\partial T$ and $\partial B_2/\partial T$ of −0.61 (H^N) and − 0.61 (N). Between the nuclei H^N and N there was a strong correlation for the pressure dependence of the temperature coefficient $\partial {C_1}^{corr}/\partial p$ with $r = 0.64$. Between the dependencies of the linear coefficients $r(\partial B_1/\partial T\text{-}\partial {C_1}^{corr}/\partial p)$ correlations of 0.64 (H^N) and 0.56 (N) were observed.

The chemical shift changes induced by high pressure lead to combined large first and second order pressure coefficients which indicate conformational changes. Generally, structures with small partial volumes are preferred at high pressures which can be observed for random-coil structures [51]. The derived combined pressure coefficients of nearly all amino acids in hIAPP become smaller with increasing temperature (see Fig. 2). This is expected when the data are corrected for random-coil effects. A complete random-coil structure should exhibit no pressure effects after the correction. This can be seen in the amino acid sequence of hIAPP for the two phenylalanine residues (F15 and F23) exhibiting nearly no pressure response. These two residues must behave exactly like sitting in the model tetrapeptides [34]. This is very interesting taking into account the information of known single point mutations either abolishing, decreasing or increasing the amyloid formation in hIAPP [43]. At this point it is remarkable that

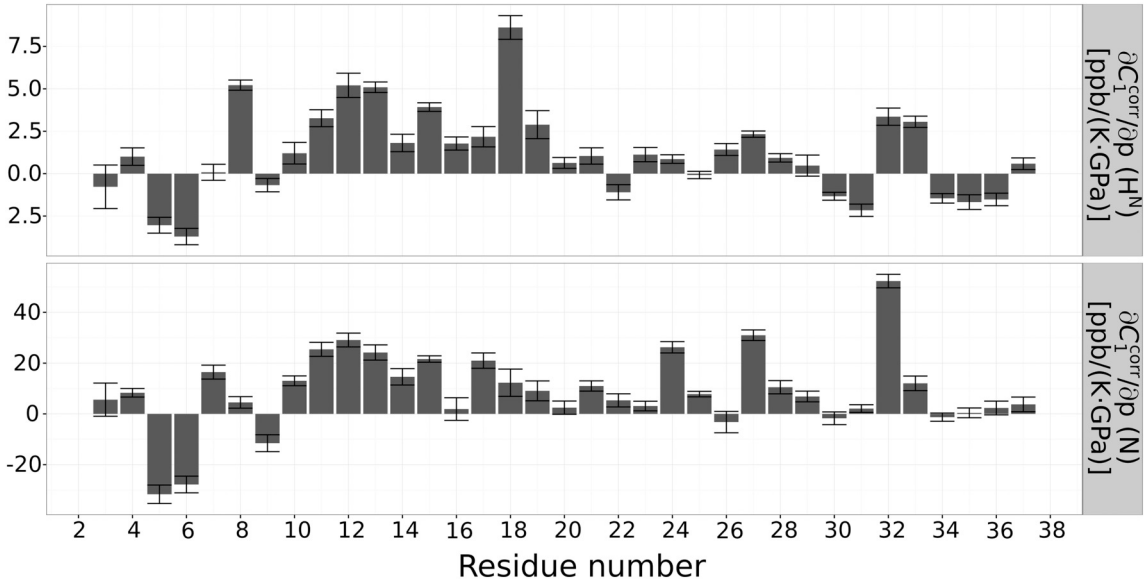

Fig. 13. Plot of the pressure dependence of the linear temperature coefficient C_1^{corr} of hIAPP(1–37). The sample contained 110 μM ^{15}N-enriched hIAPP(1–37) in 10 mM Na-acetate buffer, pH 5.5, 0.1 mM DSS in 90% ^1H_2O/10% ^2H_2O. All coefficients were corrected for random-coil effects (see Materials and Methods).

point mutations of F15 can lead to both, either an enhancement or a reduction of the propensity for amyloid formation [44,45]. The adjacent phenylalanine residues at positions 19 and 20 in the Alzheimer's Aβ peptide [49] display the opposite behavior: amino acid substitutions at these positions with increased β-sheet propensity lead to faster amyloid formation relative to amino acid substitutions with lower β-sheet propensity.

At this point it is worth to state that sequence elements of the Alzheimer β-amyloid peptide containing residues F19 and F20 show a very high homology with sequence elements of hIAPP. In case of hIAPP, these sequence elements contain the residues Q10-R11-L12-A13-N14-F15-L16 and N21-N22-F23-G24-A25-I26-L27 and in the Alzheimer β-amyloid peptide the residues Q15-K16-L17-V18-F19-F20-A21 and S26-N27-K28-G29-A30-I31-I32 (Fig. 15). In a recent extensive study we were able to demonstrate with high-pressure NMR spectroscopy that for the Alzheimer β-amyloid peptide distinct conformational states can be detected.[48] A comparison of the pressure-induced chemical shift changes based on the high sequence similarity between hIAPP and Aβ is given in Fig. 15, where we plotted the difference of the combined first and second order pressure coefficients of hIAPP and Aβ.

The N-terminal region from amino acid 3–20 displays the largest differences in the first and second order pressure coefficients between both peptides. Since hydrogen bonding largely determines the chemical shift of amide protons and nitrogens [53], large differences in first and second order pressure coefficients of combined chemical shift changes indicate pressure induced differences in hydrogen bonding patterns. Helical secondary structures contain a high amount of intra-peptide hydrogen bonds while extended β-strand structures contain a very low degree of intra-peptide hydrogen bonding. In case of the Alzheimer β-amyloid peptide, the pattern of the combined first- and second-order pressure coefficients agree very well with a solution structural model with amino acid residues 16–24 and 30–40 in extended β-strand conformation [48]. In particular, β-strand secondary structure is found for the sequence element V18-F19-F20 as predicted by the chemical shift index of the observed resonances [48]. All experimental data pinpoints to a compactly packed ensemble of Aβ in solution at ambient pressure with structural properties most probably similar to Aβ bound to polymers (extended strand conformation with internal turn). In contrast, the large differences in the first and second order pressure coefficients of the first 20 residues between hIAPP and Aβ (Fig. 15) points towards different structural ensembles in this sequence element. In this sense, Williamson and Miranker[23] found for hIAPP NMR consistent secondary chemical shifts for α-helical states for residues 5–19 based on $^1H^\alpha$, $^{13}C^\alpha$, $^{13}C'$, $^1H^N$ and $^{13}C^\beta$ NMR observable chemical shifts. Similar

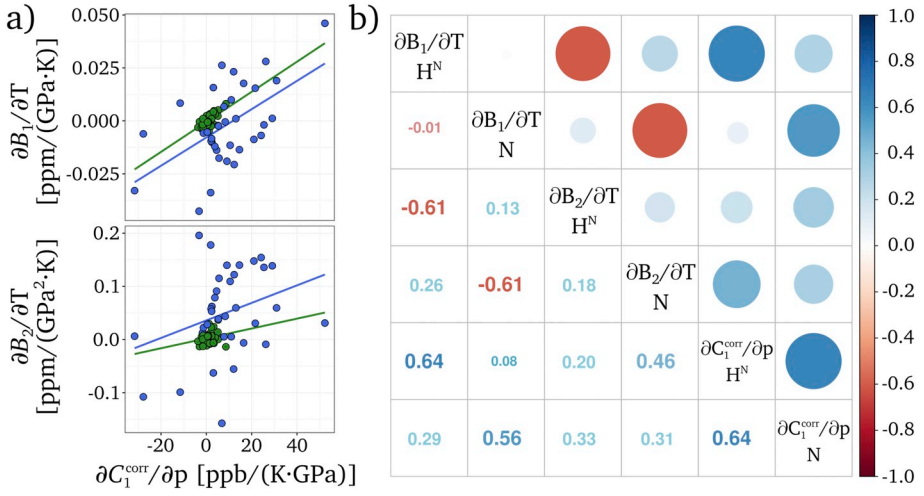

Fig. 14. Correlation analysis for the pressure dependence of the linear temperature coefficient C_1^{corr} and the temperature dependence of the combined first and second order pressure coefficients B_1 and B_2 of hIAPP(1–37). (a) Correlations for H^N (green) and N (blue) between the pressure dependent linear temperature coefficient C_1^{corr} and the temperature dependent combined first and second order pressure coefficients B_1 and B_2 of hIAPP(1–37). (b) Correlation table for the temperature and pressure dependent different coefficients and nuclei. The sample contained 110 μM ^{15}N-enriched hIAPP(1–37) in 10 mM Na-acetate buffer, pH 5.5, 0.1 mM DSS in 90% ^1H_2O/10% ^2H_2O. All coefficients were corrected for random-coil effects (see Materials and Methods). (For interpretation of the references to colour in this figure legend, the reader is referred to the web version of this article.)

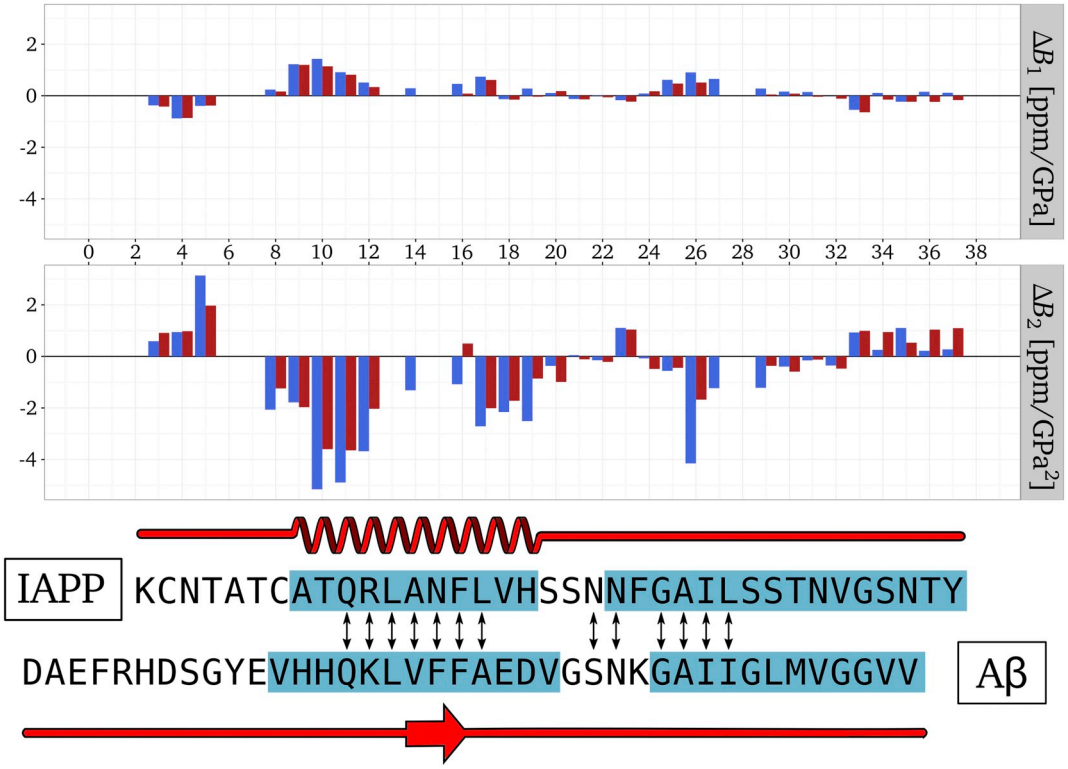

Fig. 15. Plot of the difference of the combined first and second order pressure coefficients of hIAPP(1–37) and Aβ(1–40). The IAPP sample contained 110 μM ^{15}N-enriched hIAPP(1–37) in 10 mM Na-acetate buffer, pH 5.5, 0.1 mM DSS in 90% $^{1}H_2O$/10% $^{2}H_2O$. (Top) Differences of combined first-order pressure coefficients B_1 of hIAPP(1–37) and Aβ(1–40) [48] for 278 K (blue) and 288 K (red). (Middle) Differences of combined second order coefficients B_2 of hIAPP(1–37) and Aβ(1–40) [48]. (Bottom) Sequence alignment of hIAPP and Aβ(1–40). Top red line depicts secondary shift analysis from Williamson and Miranker [23]. Bottom red line depicts CSI-analysis from Munte et al. [48] Blue boxes indicate domains suggested to be involved in self association of hIAPP [52]. Figure based on Beck Erlach et al. [38]. (For interpretation of the references to colour in this figure legend, the reader is referred to the web version of this article.)

observations are available from ion mobility coupled mass spectrometry and molecular dynamics simulations (MD), which display different possibilities of dimerization via β-loops and α-helical motifs, respectively [54,55].

Extensive simulation studies of four hIAPP variants from different species showed only a small population of the helix-coil conformation indicative for the functional role of hIAPP [56]. Differences in the combined first- and second-order pressure coefficients indicate different transient structural states in the homologous area of amino acid residues 3–20 between hIAPP and Aβ. In contrast to proteins, high hydrostatic pressure can stabilize helices in small peptides [57]. This means that the hypothetical active form of hIAPP is populated by pressure. The N-terminal region of hIAPP (residues 1–17) was shown to be very important for the initial self-association of the peptide in bulk solution [24]. The C-terminal amino acid residues 28–37 of hIAPP display no significant difference in the combined pressure coefficients compared to Aβ. This indicates a similar structural ensemble like that found in Aβ in a high-pressure NMR spectroscopic study [48]. All the results obtained by the temperature and pressure perturbation approach indicate different transient structural ensembles responsible for the initiation of the aggregation event in these two amyloidogenic peptides, hIAPP and Aβ.

In summary, monomeric hIAPP(1–37) shows NMR chemical shifts changes upon pressure and temperature changes. Higher temperatures lead to a time dependent loss of the signal intensity indicating aggregation even below the critical aggregation concentration at ambient conditions. The temperature-induced chemical shift changes can be explained by a linear model, while for the pressure-induced chemical shift changes a significant non-linear behavior is found. Especially two areas, area 1 ranging from amino acid residue 9–20, and area 2 ranging from amino acid residue 24–32, show remarkable strong pressure coefficients for the coefficients B_1 and B_2. Owing to the homologous sequence elements in the Alzheimer peptide Aβ and hIAPP we were able to demonstrate that the homologous sequence area around amino acid residues 3–20 in hIAPP displays a strong difference of the pressure coefficients, indicating completely different transient structural conformations in this homologous sequence element of the two amyloidogenic peptides. In contrast, the additional homologous sequence area around amino acid residues 28–37 in hIAPP displays only weak differences in the pressure coefficients between both peptides, indicating similar transient structural conformations in both molecules. Knowledge of the structural nature of the highly amyloidogenic hIAPP and in particular the differences in the two homologous regions with respect to the conformational ensemble of Aβ will help understand the mechanism of peptide aggregation underlying T2DM.

Acknowledgements

We acknowledge financial support from the Deutsche Forschungsgemeinschaft (DFG FOR 1979).

References

[1] H. Frauenfelder, F. Parak, R.D. Young, Conformational substates in proteins, Annu. Rev. Biophys. Biophys. Chem. 17 (1988) 451–479.
[2] H. Frauenfelder, N.A. Alberding, A. Ansari, D. Braunstein, B.R. Cowen, M.K. Hong, I.E.T. Iben, J.B. Johnson, S. Luck, M.C. Marden, J.R. Mourant, P. Ormos, L. Reinisch, R. Scholl, A. Schulte, E. Shyamsunder, L.B. Sorensen, P.J. Steinbach, A. Xie, R.D. Young, K.T. Yue, Proteins and pressure, J. Phys. Chem. 94 (1990) 1024–1037.
[3] J.L. Silva, D. Foguel, C.A. Royer, Pressure provides new insights into protein folding, dynamics and structure, Trends Biochem. Sci. 26 (2001) 612–618.
[4] R. Ravindra, R. Winter, On the temperature-pressure free-energy landscape of proteins, ChemPhysChem 4 (2003) 359–365.

[5] J. McCoy, W.L. Hubbell, High-pressure EPR reveals conformational properties of spin-labeled proteins, Proc. Natl. Acad. Sci. U. S. A. 108 (2011) 1331–1336.
[6] M.D. Collins, C.U. Kim, S.M. Gruner, High-pressure protein crystallography and NMR to explore protein conformations, Annu. Rev. Biophys. 40 (2011) 81–98.
[7] R. Mishra, R. Winter, Cold- and pressure-induced dissociation of protein aggregates and amyloid fibrils, Angew. Chem. Int. Ed. 47 (2008) 6518–6521.
[8] H.R. Kalbitzer, M. Spoerner, P. Ganser, C. Hozsa, W. Kremer, Fundamental link between folding states and functional states of proteins, J. Am. Chem. Soc. 131 (2009) 16714–16719.
[9] S. Kapoor, G. Triola, I.R. Vetter, M. Erlkamp, H. Waldmann, R. Winter, Revealing conformational substates of lipidated N-Ras protein by pressure modulation, Proc. Natl. Acad. Sci. U. S. A. 109 (2012) 460–465.
[10] K. Akasaka, Probing conformational fluctuation of proteins by pressure perturbation, Chem. Rev. 106 (2006) 1814–1835.
[11] H. Frauenfelder, S.G. Sligar, P.G. Wolynes, The energy landscape and motions of proteins, Science 254 (1991) 1598–1603.
[12] D.W. Miller, K.A. Dill, Ligand binding to proteins: the binding landscape model, Protein Sci. 6 (1997) 2166–2179.
[13] D.D. Boehr, R. Nussinov, P.E. Wright, The role of dynamic conformational ensembles in biomolecular recognition, Nat. Chem. Bio. 5 (2009) 789–796.
[14] P. Westermark, C. Wernstedt, E. Wilander, D.W. Hayden, T.D. O'Brien, K.H. Johnson, Amyloid fibrils in human insulinoma and islets of Langerhans of the diabetic cat are derived from a neuropeptide-like protein also present in normal islet cells, Proc. Natl. Acad. Sci. U. S. A. 84 (1987) 3881–3885.
[15] D. Radovan, V. Smirnovas, R. Winter, Effect of pressure on islet amyloid polypeptide aggregation: revealing the polymorphic nature of the fibrillation process, Biochemistry 47 (2008) 6352–6360.
[16] R. Kayed, J. Bernhagen, N. Greenfield, K. Sweimeh, H. Brunner, W. Voelter, A. Kapurniotu, Conformational transitions of islet amyloid polypeptide (IAPP) in amyloid formation in vitro, J. Mol. Biol. 287 (1999) 781–796.
[17] J.D. Knight, J.A. Hebda, A.D. Miranker, Conserved and cooperative assembly of membrane-bound alpha-helical states of islet amyloid polypeptide, Biochemistry 45 (2006) 9496–9508.
[18] M.F. Engel, L. Khemtémourian, C.C. Kleijer, H.J. Meeldijk, J. Jacobs, A.J. Verkleij, B. de Kruijff, J.A. Killian, J.W. Höppener, Membrane damage by human islet amyloid polypeptide through fibril growth at the membrane, Proc. Natl. Acad. Sci. U. S. A. 105 (2008) 6033–6038.
[19] D.H.J. Lopes, A. Meister, A. Gohlke, A. Hauser, A. Blume, R. Winter, Mechanism of islet amyloid polypeptide fibrillation at lipid interfaces studied by infrared reflection absorption spectroscopy, Biophys. J. 93 (2007) 3132–3141.
[20] C.E. Higham, E.T. Jaikaran, P.E. Fraser, M. Gross, A. Clark, Preparation of synthetic human islet amyloid polypeptide (IAPP) in a stable conformation to enable study of conversion to amyloid-like fibrils, FEBS Lett. 470 (2000) 55–60.
[21] K. Weise, R. Mishra, S. Jha, D. Sellin, D. Radovan, A. Gohlke, C. Jeworrek, J. Seeliger, S. Möbitz, R. Winter, Interaction of hIAPP and its precursors with model and biological membranes, in: R. Jelinek (Ed.), Lipids and Cellular Membranes in Amyloid Diseases, Wiley-VCH Verlag, Weinheim, 2011, p. 93.
[22] S.B. Padrick, A.D. Miranker, Islet amyloid polypeptide: identification of long-range contacts and local order on the fibrillogenesis pathway, J. Mol. Biol. 308 (2001) 783–794.
[23] J.A. Williamson, A.D. Miranker, Direct detection of transient alpha-helical states in islet amyloid polypeptide, Protein Sci. 16 (2007) 110–117.
[24] R. Mishra, M. Geyer, R. Winter, NMR spectroscopic investigation of early events in IAPP amyloid fibril formation, ChemBioChem 10 (2009) 1769–1772.
[25] R. Mishra, B. Bulic, D. Sellin, S. Jha, H. Waldmann, R. Winter, Small-molecule inhibitors of islet amyloid polypeptide fibril formation, Angew. Chem. Int. Ed. 47 (2008) 4679–4682.
[26] R. Mishra, D. Sellin, D. Radovan, A. Gohlke, R. Winter, Inhibiting islet amyloid polypeptide fibril formation by the red wine compound resveratrol, ChemBioChem 10 (2009) 445–449.
[27] D.S. Raiford, C.L. Fisk, E.D. Becker, Calibration of methanol and ethylene glycol nuclear magnetic resonance thermometers, Anal. Chem. 51 (1979) 2050–2051.
[28] D.S. Wishart, C.G. Bigam, J. Yao, F. Abildgaard, H.J. Dyson, E. Oldfield, J.L. Markley, B.D. Sykes, 1H, 13C and 15N chemical shift referencing in biomolecular NMR, J. Biomol. NMR 6 (1995) 135–140.
[29] H. Yamada, Pressure-resisting glass cell for high pressure, high resolution NMR measurement, Rev. Sci. Instrum. 45 (1974) 640–642.
[30] M. Beck Erlach, C.E. Munte, W. Kremer, R. Hartl, D. Rochelt, D. Niesner, H.R. Kalbitzer, Ceramic cells for high pressure NMR spectroscopy of proteins, J. Magn. Reson. 204 (2010) 196–199.
[31] W. Gronwald, H.R. Kalbitzer, Automated structure determination of proteins by NMR spectroscopy, Prog. Nucl. Magn. Reson. Spectrosc. 44 (2004) 33–96.
[32] R Core Team, R: A language and environment for statistical computing, R Foundation for Statistical Computing, Vienna, Austria, 2019 URL https://www.Rproject.org/.
[33] W. Kremer, N. Kachel, K. Kuwata, K. Akasaka, H.R. Kalbitzer, Species-specific differences in the intermediate states of human and Syrian hamster prion protein detected by high pressure NMR spectroscopy, J. Biol. Chem. 282 (2007) 22689–22698.
[34] J. Koehler, M. Beck Erlach, E. Crusca Jr., W. Kremer, C.E. Munte, H.R. Kalbitzer, Pressure dependence of 15N chemical shifts in model peptides ac-Gly-Gly-X-Ala-NH2, Materials 5 (2012) 1774–1786.
[35] F.H. Schumann, H. Riepl, T. Maurer, W. Gronwald, K.P. Neidig, H.R. Kalbitzer, Combined chemical shift changes and amino acid specific chemical shift mapping of protein-protein interactions, J. Biomol. NMR 39 (2007) 275–289.
[36] M. Kjaergaard, S. Brander, F.M. Poulsen, Random coil chemical shift for intrinsically disordered proteins: effects of temperature and pH, J. Biomol. NMR 49 (2011) 139–149.
[37] C.T. Chen, R.A. Fine, F.J. Millero, The equation of state of pure water determined from sound speeds, J. Chem. Phys. 66 (1977) 2142–2144.
[38] M. Beck Erlach, H.R. Kalbitzer, R. Winter, W. Kremer, Conformational substates of Amyloidogenic hIAPP revealed by high pressure NMR spectroscopy, ChemistrySelect 1 (2016) 3239–3243.
[39] M. Beck Erlach, J. Koehler, E. Crusca Jr., W. Kremer, C.E. Munte, H.R. Kalbitzer, Pressure dependence of backbone chemical shifts in the model peptides ac-Gly-Gly-xxx-Ala-NH2, J. Biomol. NMR 65 (2016) 65–77.
[40] M. Beck Erlach, J. Koehler, E. Crusca Jr., C.E. Munte, M. Kainosho, W. Kremer, H.R. Kalbitzer, Pressure dependence of side chain 13C chemical shifts in model peptides ac-Gly-Gly-xxx-Ala-NH2, J. Biomol. NMR 69 (2017) 53–67.
[41] I.A. Cavini, C.E. Munte, M. Beck Erlach, T. van Groen, I. Kadish, T. Zhang, T. Ziehm, L. Nagel-Steger, J. Kutzsche, W. Kremer, D. Willbold, H.R. Kalbitzer, Inhibition of amyloid Aβ aggregation by high pressures or specific D-enantiomeric peptides, Chem. Commun. 54 (2018) 3294–3297.
[42] P. Cao, L.H. Tu, A. Abedini, O. Levsh, R. Akter, V. Patsalo, A.M. Schmidt, D.P. Raleigh, Sensitivity of amyloid formation by human islet amyloid polypeptide to mutations at residue 20, J. Mol. Biol. 421 (2012) 282–295.
[43] P. Cao, P. Marek, H. Noor, V. Patsalo, L.H. Tu, H. Wang, A. Abedini, D.P. Raleigh, Islet amyloid: from fundamental biophysics to mechanisms of cytotoxicity, FEBS Lett. 587 (2013) 1106–1118.
[44] L.H. Tu, D.P. Raleigh, The role of aromatic interactions in amyloid formation by islet amyloid polypeptide, Biochemistry 52 (2013) 333–342.
[45] J.J.W. Wiltzius, S.A. Sievers, M.R. Sawaya, D. Eisenberg, Atomic structures of IAPP (amylin) fusions suggest a mechanism for fibrillation and the role of insulin in the process, Protein Sci. 18 (2009) 1521–1530.
[46] A. Abedini, D.P. Raleigh, A critical assessment of the role of helical intermediates in amyloid formation by natively unfolded proteins and polypeptides, Protein Eng. Des. Sel. 22 (2009) 453–459.
[47] J.A. Williamson, J.P. Loria, A.D. Miranker, Helix stabilization precedes aqueous and bilayer-catalyzed fiber formation in islet amyloid polypeptide, J. Mol. Biol. 393 (2009) 383–396.
[48] C.E. Munte, M. Beck Erlach, W. Kremer, J. Koehler, H.R. Kalbitzer, Distinct conformational states of the Alzheimer β-amyloid peptide can be detected by high-pressure NMR spectroscopy, Angew. Chem. Int. Ed. 52 (2013) 8943–8947.
[49] A.H. Armstrong, J. Chen, A.F. McKoy, M.H. Hecht, Mutations that replace aromatic side chains promote aggregation of the Alzheimer's Aβ peptide, Biochemistry 50 (2011) 4058–4067.
[50] N.J. Baxter, M.P. Williamson, Temperature dependence of 1H chemical shifts in proteins, J. Biomol. NMR 9 (1997) 359–369.
[51] R. Kitahara, K. Hata, H. Li, M.P. Williamson, K. Akasaka, Pressure-induced chemical shifts as probes for conformational fluctuations in proteins, Prog. Nucl. Magn. Reson. Spectrosc. 71 (2013) 35–58.
[52] E. Andreetto, L.M. Yan, M. Tatarek-Nossol, A. Velkova, R. Frank, A. Kapurniotu, Identification of hot regions of the Abeta-IAPP interaction interface as high-affinity binding sites in both cross- and self-association, Angew. Chem. Int. Ed. 49 (2010) 3081–3085.
[53] T. Asakura, K. Taoka, M. Demura, M.P. Williamson, The relationship between amide proton chemical shifts and secondary structure in proteins, J. Biomol. NMR 6 (1995) 227–236.
[54] N.F. Dupuis, C. Wu, J.E. Shea, M.T. Bowers, Human islet amyloid polypeptide monomers form ordered beta-hairpins: a possible direct amyloidogenic precursor, J. Am. Chem. Soc. 131 (2009) 18283–18292.
[55] N.F. Dupuis, C. Wu, J.E. Shea, M.T. Bowers, The amyloid formation mechanism in human IAPP: dimers have β-strand monomer-monomer interfaces, J. Am. Chem. Soc. 133 (2011) 7240–7243.
[56] C. Wu, J.E. Shea, Structural similarities and differences between Amyloidogenic and non-Amyloidogenic islet amyloid polypeptide (IAPP) sequences and implications for the dual physiological and pathological activities of these peptides, PLoS Comput. Biol. 9 (2013) e1003211.
[57] S. Neumaier, M. Büttner, A. Bachmann, T. Kiefhaber, Transition state and ground state properties of the helix-coil transition in peptides deduced from high-pressure studies, Proc. Natl. Acad. Sci. U. S. A. 110 (2013) 20988–20993.